Available online at www.sciencedirect.com

ScienceDirect

Procedia CIRP 116 (2023) 516–521

www.elsevier.com/locate/procedia

30th CIRP Life Cycle Engineering Conference.

A Bayesian Approach to Modeling Unit Manufacturing Process Environmental Impacts using Limited Data with Case Studies on Laser Powder Bed Fusion Cumulative Energy Demand

Jiankan Liao[a], Xun Huan[a], Karl R. Haapala[b], Daniel R. Cooper[a,*]

[a]*Department of Mechanical Engineering, University of Michigan, Ann Arbor, MI 48109, USA*
[b]*School of Mechanical, Industrial, and Manufacturing Engineering, Oregon State University, Corvallis, OR 97331, USA*

* Corresponding author. Tel.: +1-734-764-1357. *E-mail address:* drcooper@umich.edu

Abstract

Informed decision-making for sustainable manufacturing requires accurate manufacturing process environmental impact models with uncertainty quantification (UQ). For emerging manufacturing technologies, there is often insufficient process data available to derive accurate data-driven models. This paper explores an alternative mechanistic modeling approach using easy-to-access data from a given machine to perform Bayesian inference and reduce the uncertainty of model parameters. First, we derive mechanistic models of the cumulative energy demand (CED) for making aluminum (AlSi10) and nylon (PA12) parts using laser powder bed fusion (L-PBF). Initial parametric uncertainty is assigned to the model inputs informed by literature reviews and interviews with industry experts. Second, we identify the most critical sources of uncertainty using variance-based global sensitivity analyses; therefore, reducing the dimension of the problem. For metal and polymer L-PBF, critical uncertainty is related to the adiabatic efficiency of the process (a measure of the efficiency with which the laser energy is used to fuse the powder) and the recoating time per layer between laser scans. Data pertinent to both of these parameters include the part geometry (height and volume) and total build time. Between three and eight data points on part geometry and build time were collected on two different L-PBF machines and Bayesian inference was performed to reduce the uncertainty of the adiabatic efficiency and recoating time per layer on each machine. This approach was validated by subsequently taking direct parameter measurements on these machines during operation. The delivered electricity uncertainty is reduced by 40-70% after performing inference, highlighting the potential to construct accurate energy and environmental impact models of manufacturing processes using small easy-to-access datasets without interfering with the operations of the manufacturing facility.

Keywords: Additive Manufacturing; Sobol indices; Bayesian inference; Power measurements; Cumulative energy demand

1. Introduction

Accurate cradle-to-gate life cycle assessment (LCA) is needed to inform part design, manufacturing process selection [1,2], and process research and development that reduces environmental impacts [3]. Unit manufacturing process (UMP) inventory data available from the literature and established life cycle inventory (LCI) databases (e.g., *ecoinvent*, [4]) typically attribute impacts for a given process class as a point value (or a distribution) per unit of mass processed. Modeled environmental impacts might vary by geography but typically only by accounting for the emissions intensity of the local electricity grid. Such models might be appropriate when estimating the scale of industry-wide impacts but could be misleading when used to make manufacturing decisions. For many processes, impacts scale poorly with the mass processed, e.g., sheet metal stamping [5], and facility-level economies of scale and tipping points introduce non-linearities to the relationship between impacts and production volume [6]. Also, process impacts can vary greatly with the settings, brand/

2212-8271
10.1016/j.procir.2023.02.087

model, and generation of the machine. These issues have led to criticism that LCIs have excessive generality and inaccurate linearities [6,7]. To mitigate these issues, we can generate high-fidelity impact models for specific UMP equipment.

To model specific equipment, machine learning (ML) approaches can be used to construct data-driven models [8]. Among many examples, Susto and co-workers applied multiple classifier ML for predictive maintenance [9], and Kim and co-workers applied dimensional reduction techniques with ML-based detection methods for identifying faulty products (silicon wafers) [10]. For additive manufacturing (AM), di Angelo and di Stefano proposed a neural network with two hidden layers to estimate build time for fused deposition modeling [11]. Qin and co-workers proposed a merged neural network structure to predict the energy consumption of a polymer laser powder bed fusion (L-PBF) system [12]. Elsewhere, Kellens and co-workers proposed a linear regression model with the features engineered based on knowledge of the process physics to estimate build time for polymer L-PBF based on real build trials [13]. Data-driven models can handle high dimensional problems; however, large training datasets are often required for making accurate predictions. For many processes, particularly emerging technologies such as AM, large datasets on a specific machine are not available and data collection is difficult without disturbing work patterns; e.g., many manufacturers have yet to implement cloud-based device level data storage [14].

Mechanistic models provide an alternative approach but typically make an idealized and inflexible model form assumption that requires tuning of many input parameters to the specific machine. For example, Yi and co-workers proposed a detailed build time and energy consumption model for metal L-PBF based on the working state of individual components; e.g., the platform motor and laser device [14]. While the model is accurate, it was tailored to the machine under study and would require recalibration if applied to other machines. Calibration requires an extensive understanding of the machine components, which limits usability. Elsewhere, Baumers and co-workers constructed a mechanistic model of build time, process energy use, and cost for metal L-PBF. Several key parameters in their model (e.g., printing time per voxel) were estimated using linear regression [15].

Using both ML and mechanistic models, uncertainty quantification (UQ) has been studied as part of AM process improvement efforts [16]; however, UQ has been neglected in environmental impact modeling of AM. Thus, in this article, our contributions are:

- Tailoring mechanistic models of cumulative energy demand (CED) to specific L-PBF machines.
- Conducting forward and inverse UQ using variance-based global sensitivity analysis and Bayesian inference, reducing uncertainty with small machine-specific datasets.

We note that Monte Carlo analysis alone has been used routinely in LCA studies (e.g., [17, 18]) to quantify the uncertainty of environmental impacts based on the uncertainty of input parameters. Bayesian inference allows the uncertainty of the environmental impacts to be quantified and updated in a mathematically rigorous manner as more data is collected [19].

2. Methods

We present a mechanistic model for predicting cradle-to-gate environmental impacts of L-PBF (Section 2.1), the initial uncertainty assigned to model inputs and parameters (Section 2.2), the application of variance-based sensitivity analysis to identify the key process uncertainty (Section 2.3), and setup of the Bayesian framework for reducing uncertainty with limited machine-specific data (Section 2.4).

2.1. A mechanistic model of impacts in L-PBF

We use a mechanistic model of the environmental impacts associated with L-PBF reported by Liao et al. [20], Eq. 1, where manufacturing environmental impacts (I) are normalized per part ($p.p.$). For simplicity, we exclude post-processing here.

$$I_{p.p.} = I_{workpiece\ p.p.} + I_{energy\ p.p.} + I_{consumables\ p.p.} + I_{capital\ equipment\ p.p.} \quad (1)$$

Previous analyses have shown environmental impacts of L-PBF are driven by electrical energy requirements [3, 20]. Therefore, we focus on $I_{energy\ p.p.}$ in Eq. 1. Derivations of other terms can be found in Appendix A. Equations 2-3 define the direct energy term.

$$I_{energy\ p.p.} = i_{electricity} W_{electricity\ p.p.} \quad (2)$$

$$W_{electricity\ p.p.} = P_0 \left(\frac{1}{N} \left\lceil \frac{N}{N_0} \right\rceil T_{warm\ up} + T_{recoat,p.p.} + T_{exposure,p.p.} \right) + P_{heat} T_{recoat,p.p.} + \frac{P_{laser} T_{exposure,p.p}}{\eta_{laser}} \quad (3)$$

Here, $i_{electricity}$ is the weighted average intrinsic impact of electricity (8.52 MJ/kWh for the U.S.) [21, 22], $W_{electricity\ p.p.}$ is the delivered electricity normalized over the batch size, N, and N_0 is the maximum number of parts nested in the machine. Electrical power is modeled in Eq. 3 as a stable baseload (P_0) across the warm-up time ($T_{warm\text{-}up}$, 0.25 h for metals and 2 h for polymers), laser-powder exposure time ($T_{exposure}$), and total recoating time (T_{recoat}). Baseload power is supplied for running equipment to support the process (e.g., control unit, gas pumps, heaters, and chiller, which is often physically separate from the machine). Additional variable power is due to process physics: P_{laser} across $T_{exposure}$ at 40% efficiency in metal L-PBF (for fiber lasers) and 10% efficiency in polymer L-PBF (for CO_2 lasers), and P_{heat} across T_{recoat} for polymer L-PBF to recoat and heat the newly laid down powder. Negligible power is required during the set-up ($T_{set\text{-}up}$) and cool-down ($T_{cool\text{-}down}$) time. This baseload plus variable power structure is common for many processes and validated for L-PBF as described by Liao et al. [20].

Equations 4-5 estimate the remaining elements in Eq. 3.

$$T_{recoat,p.p.} = \frac{1}{N} \left\lceil \frac{N}{N_0} \right\rceil \frac{H_{part} + H_0}{L_{layer}} \cdot T_{layer} \quad (4)$$

$$T_{exposure,p.p.} = M_{part} / f_0 \eta_{adiabatic} \dot{m}_{adiabatic} \quad (5)$$

Here, H_{part} is part height, L_{layer} is layer thickness, T_{layer} is the recoating time per layer, M_{part} is part mass, H_0 is the insulation layer height to prevent warping (13 mm for polymers and 0 mm for metals), and f_0 is a correction factor for support material (1 for polymers and Y for metals, where Y is the process yield).

To calculate $T_{exposure}$, we adopt the adiabatic efficiency ($\eta_{adiabatic}$) concept [23], defined as the ratio between the actual and adiabatic build rates (Eq. 6), where $\dot{m}_{adiabatic}$ is calculated assuming no heat losses to the surrounding powder and no remelting/resintering. Gutowski and co-workers found the

adiabatic efficiency for the same material is similar across different L-PBF machines. Therefore, $T_{exposure}$ depends on $\eta_{adiabatic}$, total laser power (P_{laser}), the laser-powder absorption coefficient (α_{mat}), material specific heat (c_p), melting (metals) or sintering (polymer) temperature ($Temp_m$), and chamber heating temperature ($Temp_c$, ~50°C for AlSi10 and ~170°C for PA120), and (for metals) the latent heat of melting (E_m).

$$\dot{m}_{adiabatic} = \frac{P_{laser}\alpha_{mat}}{c_p(Temp_m - Temp_c)+E_m} \quad (6)$$

Table 1 presents the properties used to calculate the exposure time for the two materials studied in this article.

Table 1: Material properties for selected materials.

Parameter	Al-Si10	PA12
Material absorption rate, α_{mat}	0.62	0.90
Specific heat, c_p	963 J/kg K	2500 J/kg K
Melting or sintering temp., $Temp_m$	613°C	180°C[1]
Typical chamber temp., $Temp_c$	50°C	170°C
Enthalpy of melting, E_m	389 kJ/kg	N/A[2]

Notes: [1]Sintering temperature for PA12. [2]For polymer L-PBF, the powder is only sintered, so the enthalpy of melt is modeled as 0 kJ/kg.

2.2. Model parameters with uncertainty

The model presented in Section 2.1 is applicable across a range of L-PBF machines; however, without prior knowledge of the part design and specific L-PBF machine settings, there is considerable uncertainty associated with the model parameters. Here, input parameters are modeled using uniform distributions reflecting knowledge only about the upper and lower bound parameter values. These bounds were derived as conservative ranges from the literature (e.g., $\eta_{adiabatic}$=3.6-8.0% for AlSi10 [23]) and validated by metal and polymer L-PBF industry experts. Table 2 presents the resulting parameter distributions.

Table 2: Initial model parameter uncertainty.

Parameter[1]	Uncertainty[2]	
	Metal L-PBF	Polymer L-PBF
Average part cross-sectional area per build[3], V_{part}/H_{part}	[10, 100] cm^2	
Recoating time per layer, T_{layer}	[0, 20] sec	[10, 30] sec
Adiabatic efficiency, $\eta_{adiabatic}$	[1%, 15%]	
Process yield, Y	[50%, 100%]	
Layer thickness, L_{layer}	[30, 90] µm	[60,180] µm
Laser power, P_{laser}	[250, 2000] W	[50, 100] W

Notes: [1]Machine baseload power (P_0) not modeled as a distribution (estimated from machine specifications). [2]Uniform distribution applied to listed parameters with interval indicating upper/lower bounds. [3]Average part cross-sectional area characterizes utilization of bed area. Larger ratio indicates higher utilization (and shorter parts for same part volume).

To demonstrate the model, we apply it to the case presented by Faludi et al. [3] in which they printed 12 small AlSi10 turbine blades using a Renishaw AM250 machine. Using Monte Carlo analysis with 10,000 samples, we generate model results based only on the part specifications, including part volume (20.62 cm^3) and height (3 cm, estimated from the image), baseload (1460 W) and laser (250 W, from machine specifications) power, and layer thickness (30 µm) from build specifications. Figure 1a (left) shows the electrical energy to print the turbine blades as measured by Faludi and co-workers, and a histogram representing our model prediction. The plot shows a left-skewed distribution with a wide 95% uncertainty band that nonetheless contains the measured energy. Figure 1a (right) shows reasonable agreement between their energy measurements and our model-predicted CED (see Appendix A for modeling of non-electricity impacts).

Similarly, we use our model to predict the electrical energy requirements and CED for two more L-PBF prints: two 0.5:1 scale AlSi10 NIST test artifacts [24] and a 2×2×1 cm PA12 cuboid produced using an SLM280 and EOSP760 machine, respectively. Material and electricity requirements were measured, allowing a comparison to the model predictions, as shown in Figs. 1b and 1c. In all cases, measurements are within the 95% uncertainty band; however, modeled uncertainty is high, compromising the effectiveness of the model as a decision-making tool. Therefore, we next identify the key sources of uncertainty in the mechanistic model to then target machine-specific data collection to reduce the uncertainty.

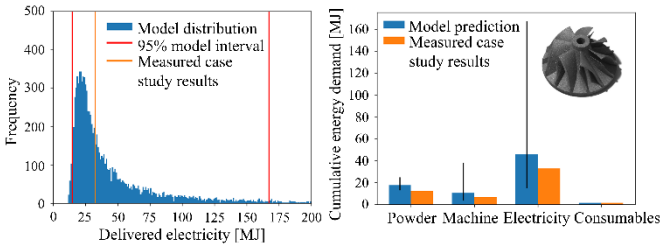

(a) Model vs. case study on a specific Renishaw AM250 machine [3]

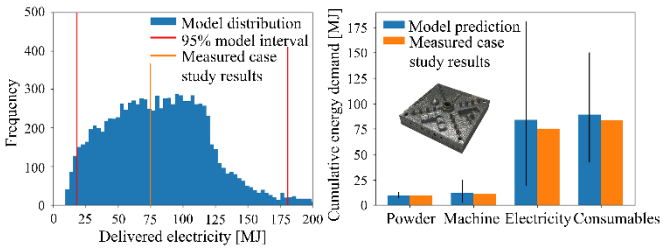

(b) Model vs. case study on a specific SLM280 machine

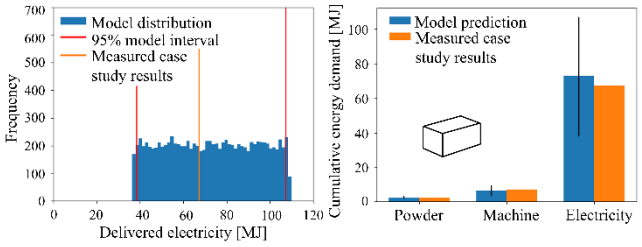

(c) Model vs. case study on a specific EOSP760 machine

Figure 1: Model results showing initial uncertainty propagation (from Table 2) vs. measured case study results. SLM280 and EOSP760 case studies conducted by the authors.

2.3. Variance-based sensitivity analysis (Sobol indices)

Figure 1 shows the model result as the propagation of the parametric uncertainty (Table 2). It is infeasible to collect high-quality data on all aspects of the processes to reduce all parametric uncertainty. Thus, we collect limited additional data guided by variance-based global sensitivity analysis [25,26] on the mechanistic model of electricity requirements with the initial parametric uncertainty shown in Table 2.

Equation 7 shows the calculation for the total effect Sobol index (S_{Ti}, [27]) of manufacturing process parameter, X_i. S_{Ti} is the fractional contribution to the total variance of the model result ($W_{electricity,p.p.}$) due to the variation of parameter X_i and any

parameters coupled with X_i (e.g., the combination between adiabatic efficiency and laser power).

$$S_{T_i} = 1 - \frac{var_{X_{\sim i}}\left(E_{X_i}(W_{electricity,p.p.}|X_{\sim i})\right)}{var(W_{electricity,p.p.})} \quad (7)$$

Here, $X_{\sim i}$ denotes the set of parameters excluding X_i. The SALib library for Python is used to numerically estimate the Sobol indices [28]. Compared with one-at-a-time (OAT) sensitivity analysis, variance-based global sensitivity analysis can explore variable interactions and dependencies [26] and can capture the uncertainty distribution of manufacturing model parameters. The model parameters with the highest resulting Sobol sensitivity indices represent the key sources of uncertainty in the model output [29] and, subsequently, become the parameters of interest for the Bayesian framework with a focus to reduce the uncertainty of those key parameters.

2.4. Bayesian inference

The model parameters of interest (θ, identified via the sensitivity analysis), together with any collected machine-specific data, y, should satisfy Bayes rule (Eqs. 8-9).

$$p(\theta|y) = \frac{p(y|\theta)p(\theta)}{p(y)} \quad (8)$$

$$p(\theta|y) \propto p(y|\theta)p(\theta) \quad (9)$$

Here, $p(\theta)$ is the prior distribution for the corresponding θs from Table 2, $p(\theta|y)$ is the posterior distribution, $p(y|\theta)$ is the likelihood distribution, and $p(y)$ is the evidence term acting as a normalizing constant. The unnormalized posterior (Eq. 9) can be derived by dropping the normalization term, $p(y)$.

The likelihood $p(y|\theta)$ provides a probabilistic measure on the mismatch between the collected data, y, and the prediction from the build time model, $T_{build}(\theta)$, equal to the sum of the total recoating and exposure times. Relative error (ε) between the collected data and model prediction (i.e., $y=T_{build}(\theta)\cdot(1+\varepsilon)$, see Eq. 10), is modeled as a normal distribution centered at zero, with a standard distribution equal to 20% of the measurement value ($\varepsilon \sim N(0,0.2^2)$). This likelihood is based on a conservative estimate of the least root mean square error by fitting the build time model to the manufacturing data collected in Table 3.

$$T_{build} = N\left(T_{recoat,p.p} + T_{exposure,p.p}\right) \quad (10)$$

For a low dimensional problem such as the problem presented here, the sample space can be divided into equally spaced grid points. The unnormalized posterior (Eq. 9) can then be derived analytically at each grid point. The trapezoidal rule is applied to numerically estimate the area (for the 1-D problem) or the volume (for the 2-D problem) under the posterior over the sample space. The unnormalized posterior can then be normalized using the estimated area or volume.

3. Results

The Sobol indices results are presented in Section 3.1, the data collected on specific machines and subsequent Bayesian inference are presented in Sections 3.2 and 3.3, respectively, and the uncertainty reduction in the model-predicted electricity requirements is presented in Section 3.4.

3.1. Global variance-based sensitivity analysis

Figure 2 shows the Sobol indices for the six selected parameters featured in the mechanistic model: average cross-sectional area, recoating time per layer, adiabatic efficiency, process yield, layer thickness, and laser power. The sensitivity analysis is based on printing a single 300 cm^3 part. This part volume is analogous to printing a 3-cm tall part with an average cross-sectional area of 100 cm^2, based on the height of the parts printed in two of the case studies in Section 2.2 and the upper-bound of the uncertainty of the cross-sectional area in Table 2.

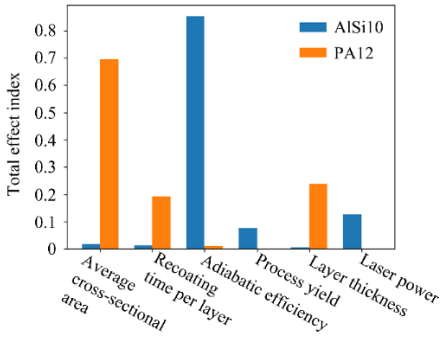

Figure 2: Global variance-based sensitivity analysis (measured as total effect indices, S_{Ti}) of key process parameters on predicted electricity requirements

Figure 2 shows adiabatic efficiency ($\eta_{adiabatic}$) has the highest sensitivity for metal L-PBF; whereas, for polymer L-PBF, average cross-sectional area, layer thickness, and recoating time per layer have the greatest effect. The dominance of total recoating time in determining polymer L-PBF impacts [18] explains the related Sobol indices results: for a fixed volume, varying the average cross-sectional area changes the part height which, alongside the layer thickness, determines the number of layers which in turn, alongside the recoating time per layer, determines the total recoating time. Based on these results, we select *recoating time per layer* and *adiabatic efficiency* as the key parameters of interest. Next, we collect data pertinent to these parameters from two L-PBF machines (one metal and one polymer) to show how Bayesian inference can be used to reduce the model uncertainty for specific machines.

3.2. Data collection for inference

Table 3 summarizes the collected data.

Table 3: Manufacturing data collected for two specific machines.

AlSi10 Build Sheet	Part geometry		Batch size, N	Parts nested, N_0	Build time, T_{build} [min]
	Volume, V_{part} [cm^3]	Height, H_{part} [cm]			
SLM280 - 1	12.73	3.06	2	2	109
SLM280 - 2	57.09	3.91	2	2	448
SLM280 - 3	6.46	3.06	4	4	283
PA12 Build Sheet	**Volume, V_{part} [cm^3]**	**Height, H_{part} [cm]**	**Batch size, N**	**Parts nested, N_0**	**Build time, T_{build} [min]**
EOSP760 - 1	4293	48.2	1	1	1590
EOSP760 - 2	1473	17.8	1	1	630
EOSP760 - 3	5379	45.2	1	1	1200
EOSP760 - 4	10156	41.7	1	1	1980
EOSP760 - 5	7692	51.7	1	1	1920
EOSP760 - 6	3424	43.4	1	1	1380
EOSP760 - 7	3338	45.6	1	1	1800
EOSP760 - 8	49273	55.2	1	1	4680

Machine-specific build data that were easy to collect were acquired from two industrial collaborators. These datasets comprised build sheets that describe single prints performed on the two machines. Each build sheet describes the total volume of the part, the maximum height of the part, the layer thickness, the laser power setting, and the build time. Three build sheets were acquired for a specific SLM280 machine printing AlSi10 and eight build sheets for a specific EOSP760 machine printing PA12.

3.3. Bayesian inference to reduce uncertainty

Figure 3 shows the Bayesian inference prior and posterior contour results for *adiabatic efficiency* and *recoating time per layer* for the two machines for which data were collected.

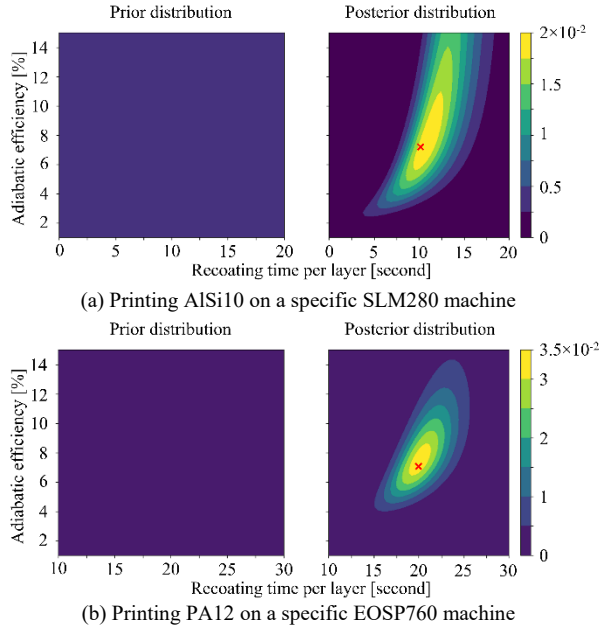

(a) Printing AlSi10 on a specific SLM280 machine

(b) Printing PA12 on a specific EOSP760 machine

Figure 3: Prior (Table 2) and posterior probability density functions (PDFs) for the manufacturing process parameter joint distribution.

The posteriors show: (1) For the SLM280 machine, a region of highest probability around $\eta_{adiabatic}$=8% and a recoating time per layer of 11 s, and (2) For the EOSP760 machine, a region of highest probability around $\eta_{adiabatic}$=7.5% and recoating time per layer of 20 s. To validate these results, we conducted case studies to calculate the CED associated with printing an AlSi10 NIST artifact and a PA12 cuboid on the same specific machines (Figs. 1b and 1c). In these studies, we measured electrical power during the build using a three-phase power meter (Fluke 435ii), allowing direct measurement of recoating time per layer and indirect calculation of adiabatic efficiency (Eq. 6). Figure 4 presents measured power for the SLM machine, showing a recoating time per layer of ~10 s and a calculated adiabatic efficiency of ~7% (marked by a red cross in Fig. 3a). For the EOS machine, a recoating time per layer of ~20 s and an adiabatic efficiency of ~7% (marked by a red cross in Fig. 3b) were found. Therefore, the hotspots within the posterior results in Fig. 3 correctly identified the likely adiabatic efficiency and recoating time per layer for these specific machines.

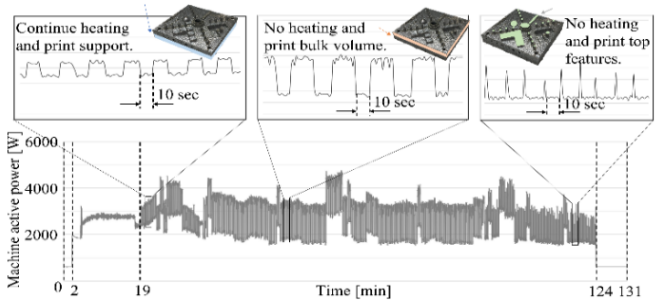

Figure 4: Electrical power measurement on the SLM280 machine.

3.4. Uncertainty reduction

The posterior uncertainty on the adiabatic efficiency and recoating time per layer shown in Fig. 3 can be adopted to recalculate the model-predicted electricity requirements and CED shown in Figs. 1b and 1c. Figure 5 shows the uncertainty reduction before and after inference on the modeled electricity requirements for printing the AlSi10 NIST artifact and PA12 cuboid. The 95% confidence interval has been reduced by 70% and 40% for the SLM280 and EOS machines, respectively.

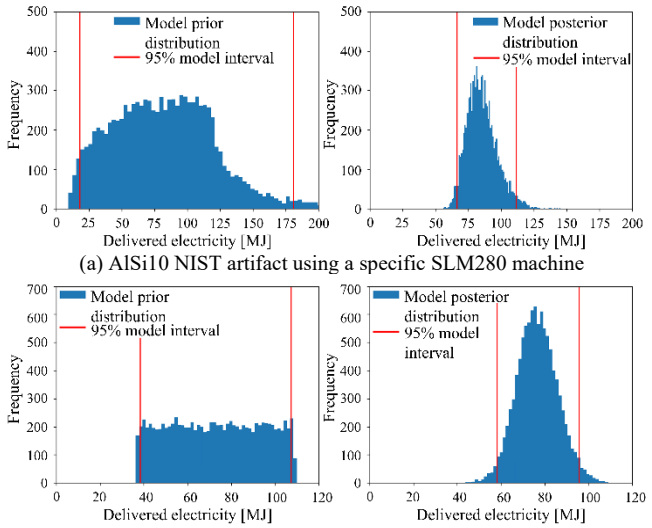

(a) AlSi10 NIST artifact using a specific SLM280 machine

(b) PA12 cuboid using a specific EOSP760 machine

Figure 5: Uncertainty quantification and reduction with Bayesian inference on the modeled electricity requirements.

4. Discussion

Informed decision-making for sustainable manufacturing requires accurate models of manufacturing process environmental impacts with UQ. Such accuracy likely requires tailoring of models to specific machines using device-level data. This work shows how using even a few easy-to-collect data points for a specific machine can reduce the uncertainty of calculated cradle-to-gate CED. Figure 6 shows how Bayesian inference reduces CED uncertainty for the NIST artifact and the PA12 cuboid. Inference shifts the CED mean from 194 to 200 MJ (+3%) for the NIST artifact and from 81 to 85 MJ (+5%) for the PA12 cuboid. For the NIST artifact, the CED upper bound reduces from 90% greater than the mean before inference to ~30% greater afterwards. For the PA12 cuboid, the CED upper bound reduces from 45% greater than the mean

before inference to less than 30% greater afterwards. This reduced uncertainty can facilitate greater confidence in sustainable process selection. Our approach can be readily applied to assess other environmental impacts, such as global warming potential, which tends to correlate with CED [30].

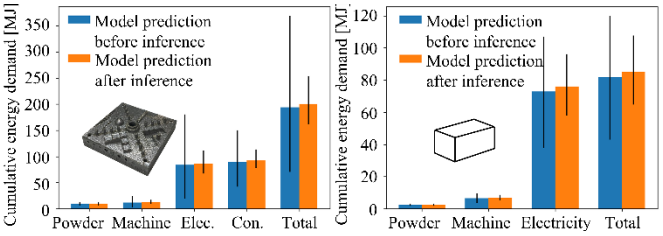

Figure 6: Breakdown of cradle-to-gate CED (with uncertainty) for the SLM280 (left) and EOSP760 (right) machine case studies.

The Bayesian approach is particularly useful for sequential learning of the manufacturing parameters when limited data are available but a prior understanding of the model form and parameter values exists. Here, the Bayesian approach has been limited to reducing the parametric uncertainty of a mechanistic model of L-PBF as new part build data is acquired; however, Bayes factor could similarly be used to discriminate between different model structures with the probability of the different model structures being updated as more build data is collected. Similarly, with more data points there is the potential to model data noise on measurements as a random variable to be learned through Bayesian inference [31].

The Bayesian approach is limited to using data collected on the same machine processing the same material using the same machine settings. However, this is often the case in industry where a single powder material is only used on a given L-PBF machine and consistent settings are established (by the machine manufacturer or user) to increase part quality. Furthermore, changes to the settings can be spotted using this Bayesian approach as that change will likely represent a radical shift in the high probability region of the posterior distribution.

Global variance-based sensitivity analysis has been used to identify the key parametric uncertainty and reduce the dimension of the problem. This approach can also help guide research and development. For example, for metal L-PBF, adiabatic efficiency has by far the largest impact on process electricity requirements. This suggests that to reduce the impacts of metal L-PBF, the focus should be on optimizing the laser melting process to reduce remelting, improving the adiabatic efficiency. In contrast, for polymer L-PBF, the part cross-sectional area has the largest impact on the electricity requirement followed by layer thickness and recoating time per layer. Based on this finding, practitioners can in turn modify the design of the part so that more can be nested in one build, minimizing the number of layers required to finish all the parts.

Acknowledgements

The first author was supported by a Ford Motor Company award. The first, second, and last authors were supported by the National Science Foundation under Grant No. #2040013.

Appendix A. Environmental impact model for L-PBF

Please see https://remade.engin.umich.edu/UQ_UMP.pdf.

References

[1] Franco, A., & Romoli, L. (2012). Charact. of laser energy cons. in sintering of polymer based powders. J. of Mat. Process. Tech., 212(4), 917–926.
[2] Huang, R., Riddle, M. E., …, & Masanet, E. (2017). Env. & Econ. Implications of Distributed Add. Manuf.. J. of Ind. Ecol., 21, S130–143.
[3] Faludi, J., Baumers, M., ..., & Hague, R. (2017). Env. Impacts of Selective Laser Melting: [What] Dominates? J. of Ind. Ecol., 21, S144–156.
[4] Ecoinvent. (2016). Cum. energy database. Ecoinvent. www.ecoinvent.org.
[5] Cooper, D.R., Rossie, K.E., & Gutowski, T.G. (2017). An Env. & cost analysis of stamp. sheet metal parts. J. Manuf. Sci. Eng. 2017, 139(4)
[6] Rossie, K. E. (2015). Thesis: An Energy and Env. Analysis of Aerospace Sheet Metal Part Manufacturing. Dep. of Mechanical Engineering. MIT
[7] Heijungs, R. (2020). Is mainstream LCA linear? Int J LCA, 25, 1872–1882.
[8] Wuest, T., Weimer, D., ..., & Thoben, K. D. (2016). Machine learning in manuf. Production and Manufacturing Research, 4(1), 23–45.
[9] Susto, G. A., Schirru, A., …, & Beghi, A. (2015). Machine learning for pred. maintenance. IEEE Trans. on Industrial Informatics, 11(3), 812–820.
[10] Kim, D., Kang, P., ., & Doh, S. (2012). Mach. learning [] for faulty wafer detection in semicon. manuf. Expert Systems with App., 39(4), 4075–4083.
[11] di Angelo, L., & di Stefano, P. (2011). A neural net.-based build time estim. for manuf. objects. Int. J. of Adv. Manuf. Tech., 57(1-4), 215-224.
[12] Qin, J., Liu, Y., & Grosvenor, R. (2018). Multi-source data analytics for AM energy cons. prediction. Advanced Eng. Informatics, 38, 840–850.
[13] Kellens, K., Yasa, E., ..., & Duflou, J. R. (2010). Env. Assess. of Sel. Laser Melt. & Sel. Laser Sint. Green-CARE Innov. Wien, Aus., 8-11.11.2010.
[14] Yi, L., Glatt, M., …, & Aurich, J. C. (2020). A method for energy model. & sim. Implem. of machine tools of selective laser melt. J. of Cleaner Prod.
[15] Baumers, M., Tuck, C.,..., & Hague, R. (2013). Transp. Built-in: Energy Cons. & Cost Estimation for Add. Manuf.. J. of Ind. Eco., 17(3), 418–431.
[16] Mahadevan, S., Nath, P., & Hu, Z. (2022). UQ for Add. Manuf. Process Impr: Recent Adv. J. of Risk & Unc. in Eng. Systems, B: Mech. Eng., 8(1).
[17] Heijungs, R. (2020). On the number of Monte Carlo runs in comparative probabilistic LCA. International J. of LCA, 25(2), 394–402.
[18] Cooper, D. R., & Gutowski, T. G. (2018). Prosp. Env. Analy. of Emerging Tech.: A [] Case Study on ISF. J. of Ind. Ecol., 24(1), 38–51.
[19] Lo, S. C., Ma, H. W., & Lo, S. L. (2005). Quantify. and reduc. uncer. in LCA using Bayesian MC method. Sci. of Tot. Env., 340(1–3), 23–33.
[20] Liao, J., …, & Cooper, D. R. (2023). The Sust. Choice? Env. Impact Model. of L-PBF & Comp. Processes. [Submitted].
[21] Argonne National Laboratory. (2021). GREET. https://greet.es.anl.gov/
[22] U.S. Energy Information Administration. (2021). Annual Energy Outlook 2021. https://www.eia.gov/outlooks/aeo/
[24] Gutowski, T., Jiang, S., Cooper, D.R., …, & Sekulic, D. P. (2017). Note on Rate & Energy Eff. Limits for Add. Manuf. J. of Ind. Ecol., 21, S69–79.
[24] Moylan, S., Slotwinski, J., …, & Alkan Donmez, M. (2012). Proposal for a Stand. Test Artifact for AM Machines & Processes. NIST
[25] Saltelli, A., Ratto, M., Andres, T., Campolongo, F., ..., & Tarantola, S. (2008). Global Sensitivity Analysis : the Primer. John Wiley.
[26] Saltelli, A., Annoni, P., …, & Tarantola, S. (2010). Variance based sens. analysis of model output. Computer Physics Communications, 181(2).
[27] Homma, T., & Saltelli, A. (1996). Importance measures in global sensit. analysis of nonlinear models. In Relia. Eng. and Sys. Safety (Vol. 52).
[28] Herman, J., & Usher, W. (2017). SALib: An open-source Python library for Sensitivity Analysis. The Journal of Open Source Software, 2(9), 97.
[29] Sobol, I. M. (2001). Global sensi. indices for nonlinear models & their Monte Carlo estimates. Math. & Computers in Sim., 55(1–3), 271–280.
[30] Ashby, M. F. (2012). Materials and the Environment: Eco-informed Material Choice, Edition 2 (2nd ed.). Oxford, UK: Elsevier.
[31] Dong, J., Liao, J., Huan, X., Cooper, D. R. (2023). Expert Elici. & Data Noise Learning for MFA using Bayesian Inference. Sub. to J. of Ind. Ecol.